A Multibody Model of the Spine for Injury Prediction in High-Rate Vertical Loading

Lucas Low, Nicolas Newell, Spyros Masouros

Abstract Underbody blast (UBB) results in lumbar spine injuries in 35% of military-vehicle casualties, resulting in disability and reduced quality of life. A multibody model of a lab-simulated UBB on a full-body cadaver was developed using geometric and inertial properties acquired from a CT scan of the same cadaver. The model comprises a skull, individual vertebral bodies, and a sacrum. Vertebral levels were connected by spring-dampers. Stiffness and damping values were taken from literature of the intervertebral disc and optimized to calibrate the model. The sacrum acceleration recorded in the experiment was input to the model sacrum, and the optimization algorithm worked to maximize the CORA (ISO18571) score of the head and T1 vertebra axial acceleration. The peak accelerations at T1 in the experiment and optimized model were 128 g and 111 g and the times-to-peak were 13.8 ms and 13.9 ms, respectively. The CORA score of both the head and T1 was 0.645 (fair). Stiffness in flexion increased by two orders of magnitude, while other degrees of freedom were scaled by values <100. This study developed a simple, fast-running, subject-specific model to predict injury across the spine. The vision is to assess the probability of injury of any seat configuration, in any vehicle.

Keywords Underbody blast, Multibody modelling, Spine biomechanics, Spine injury.

I. INTRODUCTION

Injury to the spine is a common result of high-rate axial loading, such as in an underbody blast (UBB) event to seated vehicle occupants, resulting in disability and reduced quality of life. Among individuals injured or killed in UBB events, up to 4% present fractures in the cervical spine [1-2], 21% in the thoracic spine [1-3] and 35% in the lumbar spine [1-3]. These spinal injuries predominantly occur because of compression, compression-flexion or compression-extension loading [1][3]. Fractures in the transverse processes were found to be symmetric, indicating lateral bending was not a significant contribution to injury in UBB [4]. The location of injury in the spine has been shown to be correlated with the severity of injury overall, with occupants killed by UBB showing a greater incidence of spinal injuries in the torso and neck, and isolated transverse process fractures in the lumbar spine [4-5]. Thus, studying the kinematics of the spine in UBB can aid in the development of injury-mitigation technologies to reduce mortality and morbidity in UBB.

The blast pulse has been reported to reach the pelvis and lumbar spine within 30 ms, with a peak upwards acceleration at the seat exceeding 100 g [6]. Insight into the load transfer and kinematics of the spine during high-rate loading is key to developing targeted and effective injury-mitigating strategies.

Human body models (HBMs) are common in the automotive industry for predicting injury and designing injury mitigation technologies [6-15]. However, these models were developed with the civilian automotive setting in mind and so have not been validated for the axial loading seen in UBB. Furthermore, most are finite-element (FE) models, which are complex to modify and computationally intensive.

Simpler and faster running rigid or multibody models have been used previously to study the behavior of the spine in high-rate axial loading such as simulating the Hybrid III anthropometric test device (ATD) in MADYMO under UBB and aircraft ejection scenarios [16-19]. However, the Hybrid III ATD has been shown to be inappropriate for simulating the behaviour of the human body in UBB [1][21]. Naveen *et al.* [22] developed a 2D model of the thoracolumbar spine with three degrees of freedom in the sagittal plane. This model was used to study the effect of posture on total compression of the thoracolumbar spine but has not been validated against experiments. Bosch *et al.* [23] used the MADYMO HBM, which was validated for frontal and lateral impacts only,

L. Low (e-mail: lucas.low15@imperial.ac.uk) is a PhD student in the Centre for Blast Injury Studies, S. Masouros is Reader and N. Newell is a Lecturer, all at the Department of Bioengineering at Imperial College London, UK.

in an UBB setting by optimizing the contact properties between the model and the seat and floorpan to match the kinematics of the pelvis and spine to cadaveric testing. This approach required separate models to be developed for different inputs.

Overall, a simple, quick-running multibody model of the spine that can simulate UBB could offer a practical aid to mitigation efforts. The vision is for the spine model to be valid for use with any high-rate loading pulse. The model will be easy to modify to simulate mitigation strategies and run almost 'real-time'. As such, it will allow the assessment of various injury-mitigation measures, such as seat cushions, and the effect of posture, sex and patient-specific geometries on spinal injury.

This study aims to develop a subject-specific multibody model of the spine against lab-simulated UBB testing on a whole-body cadaver in order to estimate the probability of injury during any UBB event so that the efficacy of injury-mitigation technologies, in any seating configuration, in any vehicle, can be assessed.

II. METHODS

A multibody model (Fig. 1) of a lab-simulated UBB on a full-body cadaver – Test 1.6 conducted by Bailey *et al.* [5] – was developed, using geometric and inertial properties acquired from a CT scan of the same cadaver. The head and torso were recreated in the model, which comprises rigid bodies of the skull, individual vertebral bodies (VB) of the spine, and a sacrum. Each rigid body acts as a lumped mass of the soft tissue in an axial slice of the torso at the level of the skull, vertebra or sacrum. The height of each vertebral level is the vertical distance between the superior end plates of adjacent VBs, measured at the midpoint of the functional spinal unit (FSU) in the sagittal and coronal planes. The area of the slice was approximated to be uniform across its height and was measured from the perimeter of the soft tissue at the superior endplate of the VB, without including empty space in the lungs. The mass of each slice of the torso was calculated as the volume of the slice measured from the CT scan, multiplied by the average density of soft tissue from the literature (1050 kg/m^3) [24]. By treating the torso as having a uniform density, the centre of mass coincided with the centroid of the level, calculated using geometric decomposition.

Adjacent bony structures were connected by a six degree-of-freedom spring-damper system at the centre of rotation of each FSU. This was placed on the top surface of the inferior VB, at the midplane in the coronal plane, and approximately one-third of the width from its posterior corner [25-26]. Stiffness and damping values were taken from experiments of the intervertebral disc under quasi-static loading. Stiffness was inputted as a force-displacement or moment-rotation relationship, using a polynomial fit of force-displacement and moment-rotation plots reported in the literature (Fig. 2 and Fig. 3) [27-36]. The polynomial fit was calculated from plots which contained both directions of loading in a given degree-of-freedom, and approximately in the center of the range of variation of stiffnesses. A translational damping of 1 N s/mm and a rotational damping of 2300 N mm s/rad was specified [37].

Each stiffness and damping value were modified by a separate linear scaling factor to account for the increase in stiffness of the disc at dynamic strain rates [27-28] seen in UBB, and to include the combined effects of the ligaments and soft tissue. Mass was also given a linear scaling factor to allow for studying the effect of mass recruitment on the behaviour of the model. Within each region of the spine – cervical, thoracic and lumbar – the same set of scaling factors was applied to stiffnesses, damping and mass. This resulted in three sets of scaling factors in total.

The linear scaling factors were then optimized using the Nelder-Mead Simplex algorithm to calibrate the model against a full-body laboratory-simulated UBB dataset. This algorithm is a direct search method, which does not require knowledge of the objective function or its derivative. It only needs to compare the result of the objective function, calculated from the output from each iteration of the simulation. It may also expand the search area to identify a local minimum, so prior estimation of the converged solution to apply a preset search range is not required. The sacrum acceleration recorded in Test 1.6 [5] was inputted to the model sacrum (Fig. 1). The optimization algorithm worked to maximize the CORA (ISO18571) score of the head and the first peak in the T1 vertebra axial acceleration. As the Nelder-Mead Simplex algorithm may converge to local minima and non-stationary points rather than the global minimum, different starting simplexes were sampled and optimized to identify the solution with the highest final CORA score. The Latin Hypercube design-of-experiments algorithm was used to generate 1000 initial simplexes with a scaling factor of between 1-100 for stiffness and between 1-10 for mass and damping. The 5 simplexes with the highest CORA score were then used for the optimization. A penalty function was applied to prevent negative scaling by setting a minimum scaling factor of 0.1. It was considered converged when the CORA score did not show a change greater than 0.001 within 10 iterations. The simulation in the simplex with the highest final CORA score is presented in Table II.

The experimental sacrum acceleration pulse (shown in Fig. 4) contained initial peaks under 100 g before a single peak at 180 g followed by a negative peak at -170 g. These earlier peaks are likely a result of the floor pan impacting the cadaver's lower extremities before the seat is impacted. To study the contribution of these initial peaks to the model response, the optimized model simulated a modified acceleration pulse containing only the positive and negative peaks at 180 g and -170 g (Fig. 4).

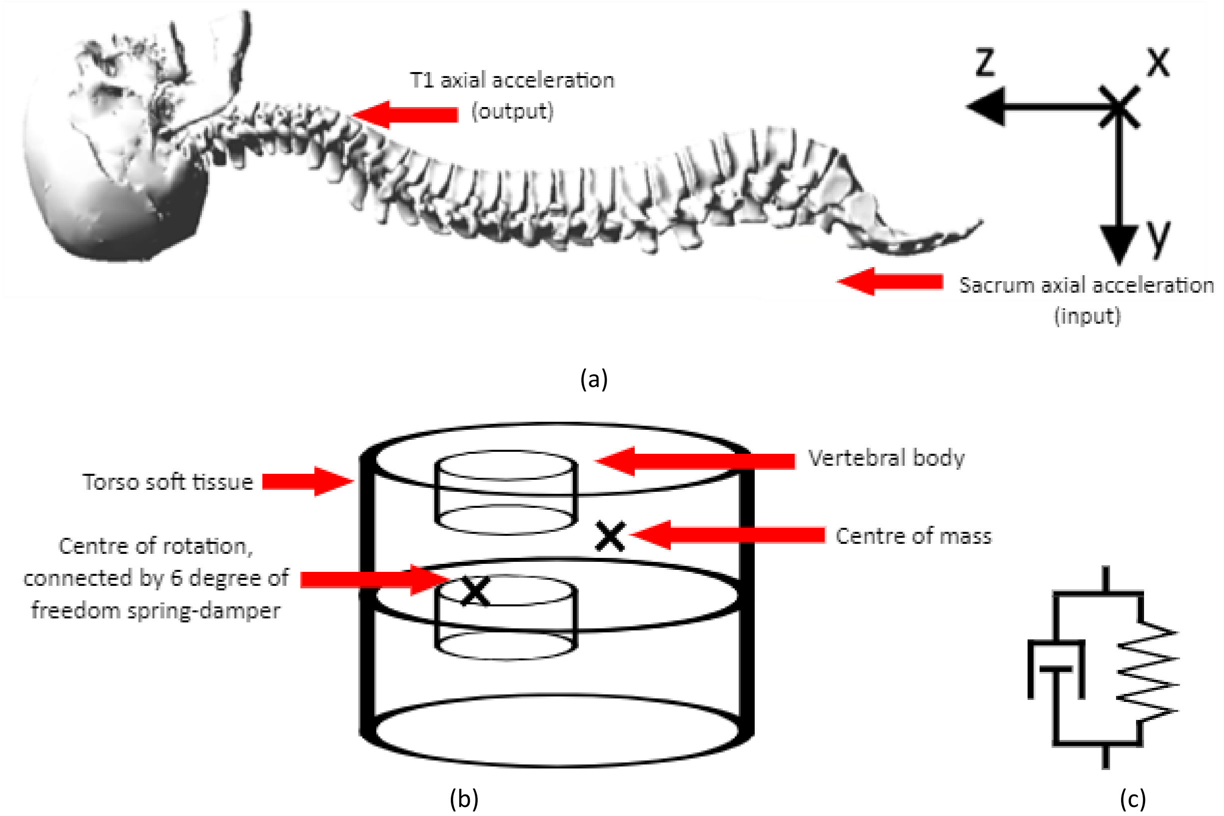

Fig. 1. (a) The multibody model is composed of rigid bodies of the skull, vertebral bodies and sacrum. The spine is positioned horizontally following the experimental setup [5]. The sacrum acceleration pulse recorded in the experiment is input to the model sacrum. The T1 acceleration is output from the model and compared with the acceleration recorded in the experiment to validate the model. The 3D representations of the skull and spine are for illustrative purposes and are not involved in the simulation. The coordinate system for the model is shown on the right. (b) Each vertebral body represents a slice of the torso. Adjacent vertebral bodies are connected by a six degree-of-freedom spring-damper element positioned at the centre of rotation of the intervertebral disc [25-26]. Each slice of the torso is treated as having uniform density and uniform cross-sectional area to calculate the location of the centre of mass by geometric decomposition. (c) Arrangement of the spring-damper system for all six degrees of freedom.

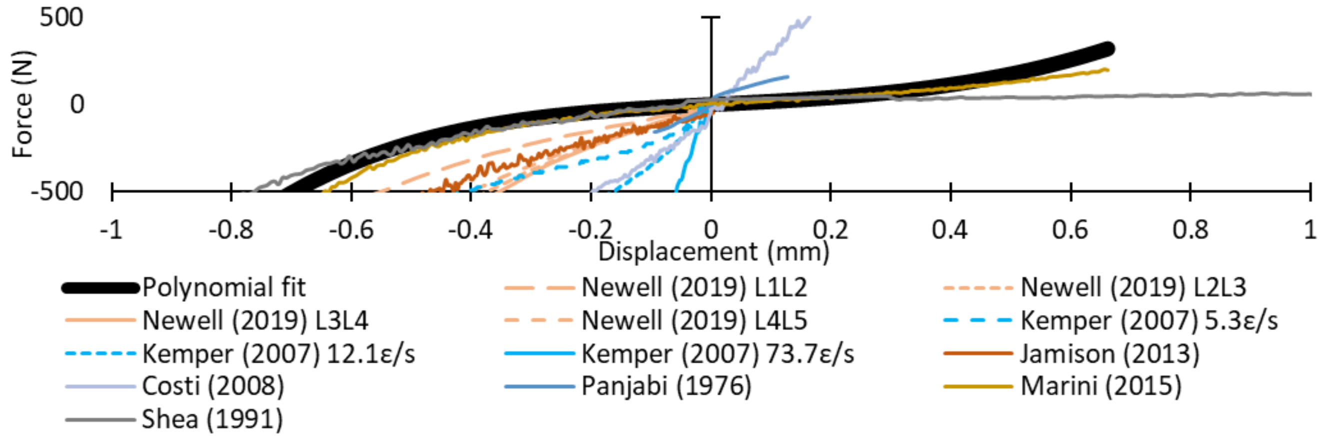

Fig. 2. Force-displacement plots for axial translation of functional spinal units (caudal-to-cranial; negative displacement indicates compression) reported in experimental studies [27-33]. The thick black line shows the polynomial fit to the plot by Marini *et al.* [32] used in the initial model.

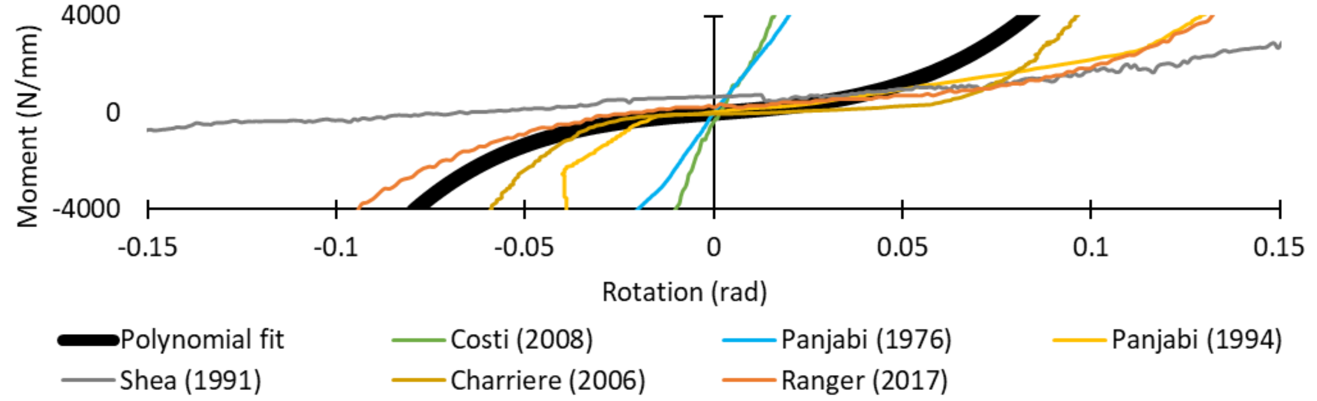

Fig. 3. Moment-rotation plots for flexion-extension of functional spinal units (positive rotation indicates flexion) reported in experimental studies [30-31][33-36]. The thick black line shows the polynomial fit to the plot by Charriere *et al*. [35] used in the initial model.

III. RESULTS

The comparison between the experiment and the model acceleration pulses is shown in Table I and Fig. 4. The scaling factors that resulted in the highest CORA score before and after optimization are shown in Table II. A typical run time to simulate 20 ms of the blast using 2000 time steps was 10 s, using a 64-bit Intel Xeon E5-2640 processor at 2.5 GHz, with 48 GB of RAM.

When optimized to the experiment, the model's stiffness in flexion-extension increased by two orders of magnitude while other degrees-of-freedom were scaled by less than 100. The translational and rotational damping values were scaled to below 1, except the thoracic translational damping (scaled by 2.5) and lumbar rotational damping (scaled by 5). The cervical and thoracic masses stayed within 50% of the nominal value, but the lumbar masses were scaled by 3.1.

TABLE I

COMPARISON BETWEEN ACCELERATION PULSES IN THE MULTIBODY MODEL AND EXPERIMENT

Sacrum input	Detail	Model	Experiment
Experimental acceleration	CORA window	0-10 ms	
	Head CORA score	0.645 (fair)	
	T1 CORA score	0.645 (fair)	
	T1 peak acceleration	111 g	128 g
	T1 time-to-peak acceleration	9.0 ms	8.9 ms
	T1 pulse width	2.5 ms	5.0 ms
Modified acceleration	CORA window	0-20 ms	
	Head CORA score	0.334 (poor)	
	T1 CORA score	0.658 (fair)	
	T1 peak acceleration	109 g	116 g
	T1 time-to-peak acceleration	12.9 ms	8.9 ms
	T1 pulse width	2.5 ms	5.0 ms

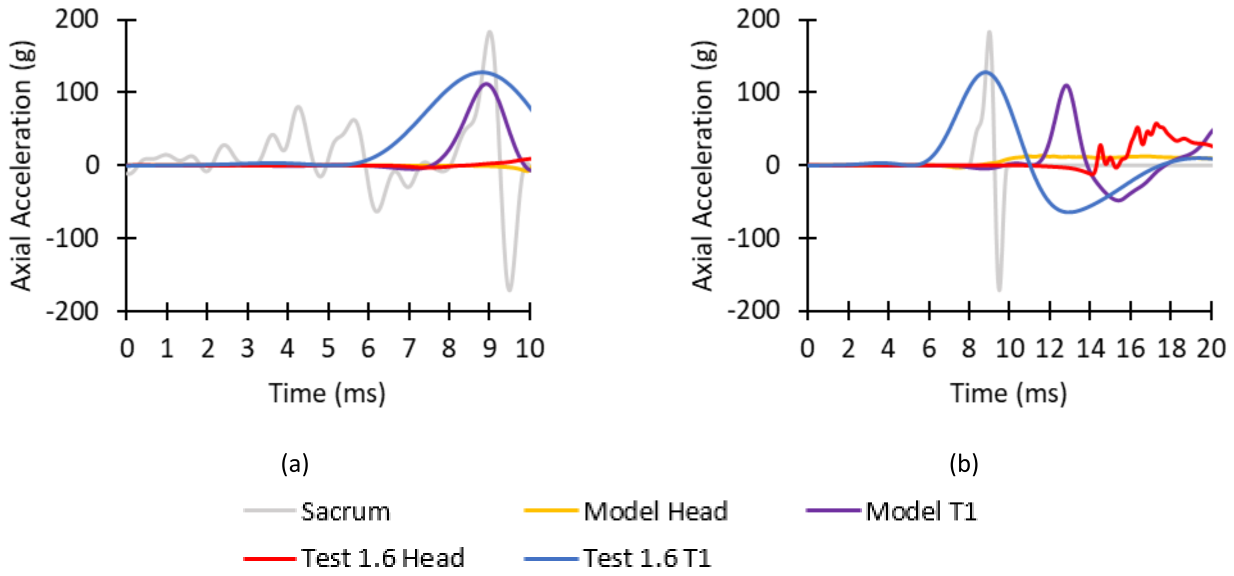

Fig. 4. Axial acceleration from the experiment (Test 1.6) [5] and model. The acceleration of the sacrum is the experimental data input to the multibody model. (a) Simulation of the experiment with the acceleration at the head and T1 vertebra as the model output. (b) Simulation of the experiment with the initial peaks removed.

TABLE II

SCALING FACTORS BEFORE AND AFTER OPTIMIZATION OF THE SIMPLEX WITH THE HIGHEST CORA SCORE

Spinal region	Parameter		Initial	Optimized	Change from Initial to Optimized (%)
Cervical	Mass		0.36	0.65	80.56
	Translational stiffness	Lateral	2.63	2.99	13.69
		Anterior-posterior	44.62	49.77	11.54
		Axial	1.34	0.25	-81.34
	Rotational stiffness	Lateral bending	70.08	74.75	6.66
		Flexion-extension	218.40	257.03	17.69
		Axial	0.39	0.60	53.85
	Translational damping		0.10	0.15	50.00
	Rotational damping		0.32	0.45	40.63
Thoracic	Mass		1.52	1.13	-25.66
	Translational stiffness	Lateral	13.70	20.42	49.05
		Anterior-posterior	31.17	30.47	-2.25
		Axial	0.26	0.1	-61.54
	Rotational stiffness	Lateral	476.06	358.98	-24.59
		Flexion-extension	4.37	3.85	-11.9
		Axial	61.93	77.49	25.13
	Translational damping		1.94	0.29	-85.05
	Rotational damping		0.15	2.52	1580.00
Lumbar	Mass		2.35	3.12	32.77
	Translational stiffness	Lateral	10.94	11.55	5.58
		Anterior-posterior	41.61	42.41	1.92
		Axial	2.16	1.60	-25.93
	Rotational stiffness	Lateral	179.01	184.74	3.20
		Flexion-extension	78.82	60.19	-23.64
		Axial	103.59	112.67	8.77
	Translational damping		0.21	0.27	28.57
	Rotational damping		5.80	5.00	-13.79

IV. DISCUSSION

A quick-running multibody model of the spine was developed and optimized to simulate a lab-simulated whole-body cadaveric UBB test. The model was able to capture the smoothing of the acceleration pulse as it propagates up the spine – from multiple peaks at the sacrum to a single peak at T1. This was found to be a benefit of using non-linear stiffnesses in the spine over linear stiffnesses [38].

The optimized model captured the magnitude and timing of the peak acceleration at the skull and T1 measured experimentally (Fig. 4(a)). However, the flexion-extension stiffness was increased significantly by two orders of magnitude. This may be partially due to the increase in stiffness of the intervertebral disc at high strain rates [27-28]. The initial stiffness values were taken from studies of the intervertebral disc in quasi-static loading due to lack of data in dynamic strain rates and rotation rates, particularly in the thoracic and cervical spines.

Over the simulated blast pulse, the strain rate was between 10-50/s and thus the scaling factor was kept constant. The mass scaling factor also did not change over the course of a single simulation as the fraction of mass recruited was assumed to be unchanged over the simulation period. The validated scaling factors will be used in future simulations of different blast pulses, using the same subject-specific model, as the strain rates are expected to be within the same order of magnitude.

Using a single point to generate reaction forces and moments, as done in this model, has been applied before [22][39-41]. Though, similar to the present study, the contributions of the facet joints, anterior and posterior ligaments, and the surrounding soft tissue to stiffness was not specific to the direction of loading. Wang *et al.* [42] implemented separate linear stiffnesses for the loading directions that are not symmetrical – flexion-extension, tension-compression and anterior-posterior translation. This would be needed to reflect the engagement of the facet joints and different ligaments in different directions of loading. A further study may be to use separate scaling factors for these non-symmetrical loading directions.

This model included only the spinal column to simplify the parameters to optimize. However, the authors appreciate that greater complexity by including other components such as the rib cage and ligaments may lead to a more representative model which would enable a greater degree of confidence when using it to assess mitigation technologies. Other multibody models of the spine have treated the thoracic region as a single rigid component due to the contribution of the ribcage to stiffness [39][42]. Huynh *et al.* [43] implemented the ribcage and ligaments as separate passive elements. Additionally, existing multibody models have included muscles as active elements [39][41-42][44]. The model developed in this study considered the muscles to have a passive stiffness due to the comparison being against a cadaveric test. The present study aimed to capture all these contributions to passive stiffness using a single scaling factor for each degree of freedom. A further development would be to implement these contributions as parallel spring-damper systems, each optimized independently.

Mass was included as a variable in the optimization in this study as preliminary models where mass was not optimized resulted in poor matches between model and experiment. Allowing mass to be varied would address that fact that each vertebral level was considered to have a uniform area across its height and uniform density. It also replicated the different amount of mass recruitment as the pulse transfers up the spine. This approach may be improved by implementing mass recruitment as a function of time rather than a constant over the 20 ms blast pulse. The optimization sequence with mass as a variable will also need to be verified by simulating additional cadaveric UBB tests.

The pulse-width in the optimized model was less than half of that seen in the experimental data. As most of the damping values were scaled to below the nominal value, this may be a result of the model being unsensitive to changes in the damping values compared to the stiffness. The model may also be unsensitive to increases in mass, as the lumbar spine mass was tripled instead of being reduced as expected to reflect the delayed mass recruitment in high-rate loading. This suggests future optimization should be completed with a time-dependent variation in mass recruitment.

The additional simulation using an acceleration pulse with a single positive and negative peak (Fig. 4(b)) was able to capture the pulse shape and magnitude beyond the first peak at T1, beyond the point the model has been calibrated. The pulse-width remained unchanged. This suggests that experimentally, the initial acceleration from impact to the lower extremities contributes to the timing of the response in the spine.

Overall, the multibody model was able to capture the peak acceleration of the T1. Other kinetic and kinematic data such as the peak axial force, peak axial acceleration of VBs, and peak compression of intervertebral discs may also be extracted from the model. These metrics have all been proposed as injury criteria [6][18][22][45-46]; thus, the results of the simulations with this model in conjunction with injury-risk curves will enable the prediction of injury at all levels of the spine. This will enable the assessment of the efficacy of injury-mitigation strategies for any seating configuration, in any vehicle.

V. CONCLUSIONS

This study developed a simple, fast-running, subject-specific model of the spine to predict injury across the spine in UBB based on the acceleration in each vertebral body. These models may quickly and inexpensively simulate a range of body dimensions, include different seats as spring-dampers, and reposition the spine without the need to modify soft tissue as well. The next step is to further refine the optimization method using data from additional cadaveric experiments. The increase in flexion stiffness of two orders of magnitude needs to be studied with flexion experiments on the intervertebral discs, from all regions of the spine, at dynamic rotation rates to determine if it is physiological, or if the model should be modified to include the facet joints and longitudinal ligaments.

VI. ACKNOWLEDGEMENTS

The Royal British Legion's funding and Dr Robert Salzar of the University of Virginia, who provided the data from full-body cadaveric testing, are kindly acknowledged.

VII. REFERENCES

[1] Danelson, K., Watkins, L., *et al.* (2018) Analysis of the Frequency and Mechanism of Injury to Warfighters in the Under-body Blast Environment. *Stapp Car Crash Journal*, **62**: pp.489–513.

[2] Alvarez, J., Epidemiology of Blast Injuries in Current Operations, *RTO-MP-HFM-207*, KN1-1:KN1-10.

[3] Loftis, K. L., Mazuchowski, E. L., Clouser, M. C., Gillich, P. J. (2019) Prominent injury types in vehicle underbody blast. *Military Medicine*, **184**: pp.261–264.

[4] Newell, N., Pearce, A. P., *et al.* (2018) Analysis of isolated transverse process fractures sustained during blast-related events. *Journal of Trauma and Acute Care Surgery*, **85**: pp.S129–S133.

[5] Vasquez, K. B., Brozoski, F. T., Logsdon, K. P., Chancey, V. C. (2018) Retrospective Analysis of Injuries in Underbody Blast Events: 2007-2010. *Military Medicine*, **183:** pp. 347-352.

[6] Bailey, A. M., Christopher, J. J., Brozoski, F., Salzar, R. S. (2015) Post Mortem Human Surrogate Injury Response of the Pelvis and Lower Extremities to Simulated Underbody Blast. *Annals of Biomedical Engineering*, **43**: pp.1907–1917.

[7] Butz, K., Spurlock, C., *et al.* (2020) Development of the CAVEMAN Human Body Model: Validation of Lower Extremity Sub-Injurious Response to Vertical Accelerative Loading. *Stapp Car Crash Journal*, **61**: pp.175–209.

[8] Lei, J., Zhu, F., Jiang, B., Wang, Z. (2018) Underbody blast effect on the pelvis and lumbar spine: A computational study. *Journal of the Mechanical Behavior of Biomedical Materials*, **79:** pp. 9-19.

[9] Somasundaram, K., Kalra, A. (2017) An Experimental and Numerical Study of Hybrid III Dummy Response to Simulated Underbody Blast Impacts. *Journal of Biomechanical Engineering*, **139:** pp. 121002-1 – 121002-12.

[10] Umale, S., Humm, J. R., Yoganandan, N. (2021) EFFECTS OF PERSONAL PROTECTIVE EQUIPMENT ON SPINAL COLUMN LOADS FROM UNDERBODY BLAST LOADING. *International Mechanical Engineering Congress and Exposition*, 2021, online.

[11] Panzer, M. B., Fice, J. B., Cronin, D. S. (2011) Cervical spine response in frontal crash. *Medical Engineering and Physics,* **33**: pp.1147–1159.

[12] Stech, E. L., Payne, P. R. (1969) Dynamics Models of the Human Body. *Aerospace Medical Research Laboratory*.

[13] Somasundaram, K., Zhang, L., *et al*. (2019) Evaluating thoracolumbar spine response during simulated underbody blast impact using a total human body finite element model. *Journal of the Mechanical Behavior of Biomedical Materials*, **100**.

[14] Iwamoto, M., Kisanuki, Y., *et al.* (2002) Development of a finite element model of the total human model for safety (THUMS) and application to injury reconstruction. *Proceedings of IRCOBI Conference*, 2002, Munich, Germany.

[15] Sugimoto, T., Yamazaki, K. (2005) First results from the JAMA human body model project. *Proceedings of 19th International Technical Conference on the Enhanced Safety of Vehicles,* 2005, Washington, D.C., USA.

[16]

[17] Boucher, H., Waagmeester, C. D. (2003) Enhanced FAA-hybrid III Numerical Dummy Model in MADYMO for Aircraft Occupant Safety Assessment. *SAE Technical Paper Series*, 2003, Montreal, Canada.

[18] Kulkarni, K., Ramalingam, J., Thyagarajan, R. (2013) Evaluating the Effectiveness of Various Blast Loading Descriptors as Occupant Injury Predictors for Underbody Blast Events. *NDIA Ground Vehicle Systems Engineering and Technology Symposium*, 2013, Troy, United States.

[19] Chandra, S., Ramalingam, J., Thyagarajan, R. (2014) REDUCED ORDER MODELING FOR RAPID SIMULATION OF BLAST EVENTS OF A MILITARY GROUND VEHICLE AND ITS OCCUPANTS. *NDIA Ground Vehicle Systems Engineering and Technology Symposium*, 2013, Novi, United States.

[20] Arepally, S. Gorsich, D., Hope, K., Gentner, S., Drotleff, K. (2008) Application of Mathematical Modeling in Potentially Survivable Blast Threats in Military Vehicles. *Proceedings of the 26th Army Science Conference*, 2008, Orlando, United States.

[21] Ott, K., Drewry, D., *et al.* (2020) Comparison of Human Surrogate Responses in Underbody Blast Loading Conditions. *Journal of Biomechanical Engineering,* **142:** pp. 091010-1 – 091010-13.

[22] Naveen, R. R., Krishnapillai, S. (2020) An improved spinal injury parameter model for underbody impulsive loading scenarios. *International Journal for Numerical Methods in Biomedical Engineering*, **36**.

[23] Bosch, K., Good, A., *et al.* (2021) Optimization of underbody blast energy-attenuating seat mechanisms using modified MADYMO human body models. *Journal of Biomechanical Engineering*, **143:** pp. 061006-1-061006-11.

[24] Erdmann, W., Gos, T. (1990) Density of Trunk Tissues of Young and Medium Age People. *Journal of Biomechanics*, **23**: pp.945–947.

[25] Pearcy, M. J., Bogdul, N. (1998) Instantaneous Axes of Rotation of the Lumbar Intervertebral Joints. *Spine*, **13**: pp.1033–1041.

[26] Amevo, B., Worth, D., Bogduk, N. (1991) Instantaneous axes of rotation of the typical cervical motion segments: a study in normal volunteers. *Clinical Biomechanics*, **6**: pp.111–117.

[27] Newell, N., Carpanen, D., Grigoriadis, G., Little, J. P., Masouros, S. D. (2019) Material properties of human lumbar intervertebral discs across strain rates. *The Spine Journal*, **19**: pp.2013–2024.

[28] Kemper, A., McNally, C., Manoogian, S., McNeely, D., Duma, S. (2007) Stiffness Properties of Human Lumbar Intervertebral Discs in Compression and the Influence of Strain Rate. *Materials Science*, **43**: pp. 176-181.

[29] Jamison, D., Cannella, M., Pierce, E. C., Marcolongo, M. S. (2013) A comparison of the human lumbar intervertebral disc mechanical response to normal and impact loading conditions. *Journal of Biomechanical Engineering*, **135**: pp.1–5.

[30] Costi, J. J., Stokes, I. A., Gardner-Morse, M. G., Iatridis, J. C. (2008) Frequency-dependent behavior of the intervertebral disc in response to each of six degree of freedom dynamic loading: Solid phase and fluid phase contributions. *Spine*, **33**: pp.1731–1738.

[31] Panjabi, M. M., Brand, R. A., White, A. A. (1976) Three-dimensional flexibility and stiffness properties of the human thoracic spine. *Journal of Biomechanics*, **9**: pp.185–192.

[32] Marini, G., Huber, G., Püschel, K., Ferguson, S. J. (2015) Nonlinear dynamics of the human lumbar intervertebral disc. *Journal of Biomechanics*, **48**(3): pp.479–488.

[33] Shea, M., Edwards, W. T., White, A. A., Hayes, W. C. (1991) Variations of stiffness and strength along the human cervical spine. *Journal of Biomechanics,* **24**: pp.95–107.

[34] Panjabi, M. M., Oxland, T. R., Yamamoto, I., Crisco, J. J. (1994) Mechanical behaviour of the human lumbar and lumbosacral spine as shown by three-dimensional load-displacement curves. *The Journal of Bone and Joint Surgery,* **76-A**: pp.413–424.

[35] Charriere, E. A., Beutler, T., *et al*. (2006) Compliance of the L5-S1 spinal unit: A comparative study between an unconstrained and a partially constrained system. *European Spine Journal,* **15**: pp.74–81.

[36] Ranger, T. A., Newell, N., Grant, C. A., Barker, P. J., Pearcy, M. J. (2017) Role of the Middle Lumbar Fascia on Spinal Mechanics. *Spine*, **42**: pp.E459–E465.

[37] Abouhossein, A., Weisse, B., Ferguson, S. J. (2010) A Multibody modelling approach to determine load sharing between passive elements of the lumbar spine. *Computer Methods in Biomechanics and Biomedical Engineering*, **14**: pp.527–537.

[38] Lucas, L., Salzar, R., Newell, N., Masouros, S. (2021) The Role of Nonlinear Stiffness in Modelling High Rate Axial Loading of the Spine. *Proceedings of IRCOBI Conference*, 2021, online.

[39] Christophy, M., Senan, N. A. F., Lotz, J. C., O'Reilly, O. M. (2012) A Musculoskeletal model for the lumbar spine. *Biomechanics and Modeling in Mechanobiology*, **11:** pp. 19-34.

[40] Keller, T. S., Colloca, C. J., Beliveau, J. (2002) Force-deformation response of the lumbar spine: a sagittal plane model of posteroanterior manipulation and mobilization. *Clinical Biomechanics*, **17:** pp. 185-196.

[41] Bruno, A. G., Bouxsein, M. L., Anderson, D. E. (2015) Development and validation of a musculoskeletal model of the fully articulated thoracolumbar spine and ribcage. *Journal of Biomechanics*, **137:**.

[42]Wang, W., Wang, D., Groote, F. D., Scheys, L., Jonkers, I. (2020) Implementation of physiological functional spinal units in a rigid-body model of the thoracolumbar spine. *Journal of Biomechanics*, **98:**.

[43]Huynh, K., Gibson, I., Jagdish, B. N., Lu, W. F. (2015) Development and validation of a discretised multi-body spine model in LifeMOD for biodynamic behaviour simulation. *Computer Methods in Biomechanics and Biomedical Engineering*, **18:** pp. 175-184.

[44]de Zee, M., Hansen, L., Wong, C., Rasmussen, J., Simonsen, E. B. (2007) A generic detailed rigid-body lumbar spine model. *Journal of Biomechanics*, **40:** pp. 1219-1227.

[45]Yoganandan, N., Chirvi, S., Pintar, F. A., Banerjee, A., Voo, L. (2018) Injury Risk Curves for the Human Cervical Spine from Inferior-to-Superior Loading. *Stapp Car Crash Journal*, **62:** pp. 271-292.

[46]Stemper, B. D., Chirvi, S., *et al.* (2018) Biomechanical Tolerance of Whole Lumbar Spines in Straightened Posture Subjected to Axial Acceleration. *Journal of Orthopaedic Research*, **36:** pp. 1747-1756.